Contrasting the roles of regional anthropogenic aerosols from the western and eastern Hemispheres in driving the 1980–2020 Pacific multi-decadal variations

Chenrui Diao[1, 2], Yangyang Xu[1, *], Aixue Hu[3], and Zhili Wang[4]

[1]Department of Atmospheric Sciences, Texas A&M University, College Station, TX, USA
[2]Department of Atmospheric Science, Colorado State University, Fort Collins, CO, USA
[3]Climate and Global Dynamics Lab, NSF National Center for Atmospheric Research, Boulder, CO, USA
[4]State Key Laboratory of Severe Weather & Key Laboratory of Atmospheric Chemistry of CMA, Chinese Academy of Meteorological Sciences, Beijing, China

Correspondence to: Yangyang Xu (yangyang.xu@tamu.edu)

Abstract. The multi-decadal variations of the Pacific climate are extensively discussed as being influenced by external forcings such as greenhouse gases (GHGs) and anthropogenic aerosols (AA). Unlike GHGs, the potential impacts of AA could be more complex because of the heterogeneity of spatial distribution during the past few decades. Here we show, using regional aerosol forcing large ensemble simulations based on CESM1, that the increasing fossil fuel-related aerosol emission over Asia (EastFF) and the reduction in aerosol emission over North America and Europe (WestFF) have remarkably different impacts in driving the Pacific circulations and SST changes since the 1980s. EastFF excites a typical El Niño-like SST pattern in the tropical Pacific and weakens the climatological Pacific Walker Circulation. WestFF induces a CP-type El Niño-like SST pattern with warming at middle region of the equatorial Pacific, which is consistent with the 2nd leading EOF pattern of the observation. Over the North Pacific region, EastFF, located at low-to-mid latitudes, favors an IPO-like SST pattern through a teleconnection pathway between tropical and extratropical Pacific but is overwhelmed by internal variability evolving from a positive phase to a negative IPO phase. In contrast, WestFF, located at mid-to-high latitudes, strongly affects the North Pacific via a west-to-east mid-latitude pathway and induces extensive warming. The competing effects of the heterogeneously distributed regional aerosol forcings are expected to be changed in the near future, which is likely to introduce opposite and more profound impacts of aerosol forcing on the Pacific multi-decadal changes.

1 Introduction

Greenhouse gases (GHGs) and Anthropogenic aerosols (AA) are two major external forcings that drive the long-term global and regional climate changes. In contrast to the GHG warming effect, AA shows a net cooling effect on the global mean temperature by scattering income shortwave radiation and affecting the cloud properties (Ramanathan et al., 2001; IPCC, 2018; Lin et al., 2018). Unlike the well-mixed GHG, the AA forcings show strong spatial heterogeneity because of the uneven distribution of emission sources and relatively short atmospheric residence time (Deser et al., 2020; Kang et al.,

2021; Diao et al., 2021). In addition, the AA forcings have also shown a non-monotonic temporal evolution. In the 1980s, the AA emissions over North America and Europe mid-latitude (hereby collectively denoted as "Western Hemisphere") reached the peak emission level and started to decrease since then due to the strengthened pollution control in the developed

35   nations. However, the ongoing industrialization over the South and East Asia low latitude regions (hereby denoted as "Eastern Hemisphere") has led to a nearly monotonic increase in AA emission over the past few decades. The opposite AA emission changes between the western and eastern Hemispheres effectively reduce the magnitude of the global total AA forcing and, more importantly, present a spatial shift mode from West to East since the 1980s (Ming and Ramaswamy, 2011; Shindell et al., 2015; Deser et al., 2020; Shao et al., 2023).

40

Because of AA forcings' complex temporal and spatial features since the 1980s, many recent efforts have been made to investigate their impacts on the global and regional climates due to the recent spatial redistribution. Shi et al. (2022) separated the climate impact of AA from GHG and internal variability based on a pattern recognition method and demonstrated that the shift mode of AA forcings has dominated the total AA effects since the 1980s. Kang et al. (2021)

45   examined the climate responses to the zonal shift (west to east) of aerosol forcing based on idealized model simulations and argued that the shift mode contributes to a La Niña-like pattern over the equatorial Pacific. However, the meridional component of AA forcing shift (from mid-latitude in the Western Hemisphere to lower latitudes in the Eastern Hemisphere) has not been closely examined. Diao et al. (2021) developed two contrasting sets of regional aerosol large ensemble simulations driven by spatially resolved historical aerosol emissions. They demonstrated the distinct roles of East versus

50   West AA forcing in driving the zonal mean tropospheric and mid-latitude circulations, emphasizing that both zonal and meridional shifts of the AA forcing are important. More recently, Xiang et al. (2023) did idealized simulations with South and East Asia forcings separated to probe the role of AA forcing shifts within the Eastern Hemisphere. Wang et al. (2024) indicated that the inhomogeneous aerosol forcing dominated the recent decadal change of summer water vapor budget over the Tibetan Plateau.

55

In addition to complex effects on atmospheric circulations and surface climate, recent studies suggested that the spatially heterogeneous and temporally non-monotonic AA forcing could also modulate oceanic variations at interannual to multi-decadal time scales, which were conventionally thought to be mainly driven by internal variability. Booth et al. (2012) argued that the decline of European AA emissions contributes to the Atlantic multidecadal variations, and such arguments have been supported by several following studies (Bellomo et al., 2018; Hua et al., 2019; Watanabe and Tatebe, 2019;

60   Hassan et al., 2021; Shi et al., 2023). However, to what extent AA forcing drives the observed Atlantic decadal variations, relative to the internal variability remains highly debated. In addition, studies have focused on the AA effects on the Pacific variations (Allen et al., 2014; Dong et al., 2014; Hua et al., 2018; Dittus et al., 2021; Meehl et al., 2021), showing that AA forcings can induce decadal variations over both tropical and extratropical Pacific. Shi et al. (2023) investigated the impact

65   of AA forcing on the North Pacific by looking at the subsurface ocean temperature responses and found unique zonal-mean

patterns, which further indicated the importance of AA forcing in the North Pacific climate. However, the mechanisms of how regional AA forcings affect the extratropical Pacific remain less investigated due to the entangled offsetting effects from East and West AA.

70   Based on the large ensemble of regional aerosol simulations conducted by Diao et al. (2021), here we aim to isolate and contrast the climate responses due to the regional aerosol forcings originating from the eastern to western Hemispheres. We untangle their offsetting effects over the tropical and extratropical Pacific (especially North Pacific), and further investigate the dynamical mechanism of how regional AA forcings remotely affect the extratropical North Pacific regions in a multi-decadal time scale.

75   **2 Methods**

2.1 Model and simulations

The model simulations in this study are based on the Community Earth System Model 1 (CESM1) fully coupled model developed by the National Center for Atmospheric Research (NCAR) and community scientists (Hurrell et al., 2013). We leverage the CESM1 large ensemble (Kay et al., 2015) and CESM1 single forcing large ensembles (Deser et al., 2020) to

80   investigate the overall climate effects of the combined external forcings (abbreviated as "ALL"), industrial aerosols (fossil-fuel-source related, abbreviated as "FF"), and biomass-burning related aerosols (abbreviated as "BMB").

In addition, considering the opposite aerosol emission trends between the eastern and western Hemispheres, two sets of large ensemble regional AA forcing simulations (Diao et al., 2021) were applied, which follows the setup of CESM1 single

85   forcing large ensemble. The regional simulations separated climate impacts induced by the increasing FF over East and South Asia ("Fix_EastFF1920" in Diao et al., 2021) and by the decreasing FF over North America and Europe ("Fix_WestFF1920" in Diao et al., 2021). Both of the regional AA forcing simulations cover 1980 to 2020 with 10 ensemble members each. The simulations follow the design of the CESM1 single forcing large ensemble; that is, fixing the AA forcing over focused regions at 1920 levels while keeping outside AA and all other external forcings evolving with time into the 21st

90   century. Thus, the climate response to the regional aerosol forcings can be isolated by subtracting the regional simulation results from "ALL" results. The difference between ALL and the two regional AA simulations are denoted as "EastFF" and "WestFF" hereafter, respectively. As an example, Figure 1a–c shows the decadal changes in aerosol optical depth (AOD) induced by EastFF, WestFF, and FF from 1980 to 2020, respectively. One note here is that the climate changes in response to FF do not necessarily equal the simple combination of that in response to EastFF and WestFF because the FF results also

95   contain anthropogenic aerosol forcings originated from other regions not covered by EastFF and WestFF (e.g., Africa and Arabian Peninsula, Fig. 1d). More details of the regional AA single forcing large ensemble simulations are described in Diao et al. (2021).

All analyses in this study are based on ensemble-averaged results of monthly outputs of the five simulations mentioned
100 above (ALL, FF, EastFF, WestFF, and BMB) to exclude the impact of internal variability in the model.

2.2 Observational data

In order to test the fingerprints of regional aerosol forcings in real-world observations, the ECMWF Reanalysis v5 (ERA5)
monthly reanalysis dataset developed by the European Centre for Medium-Range Weather Forecasts (ECMWF) is applied in
this study (Hersbach et al., 2023). ERA5 data provides global monthly sea surface temperature (SST) anomalies from 1940
105 to the present day at a 0.25° x 0.25° grid. We utilized the period of 1980 to 2020 from ERA5 to be consistent with the model
simulation coverage. To facilitate comparisons between the CESM simulations and the reanalysis results, we interpolate the
ERA5 data onto the model grid of 1° latitude x 1° latitude. We also tested another widely used SST reconstructed dataset –
the Extended Reconstructed Sea Surface Temperature (ERSST; Huang et al., 2017) – and got consistent decadal variation
patterns over the Pacific, so we only show the ERA5 results in this study.

110 ## 2.3 Metrics for Pacific decadal variations

To investigate the potential impact of regional aerosols on the Pacific decadal variations (PDV), we use the conventional
definition of the Interdecadal Pacific Oscillation (IPO) index as the leading empirical orthogonal function (EOF) of the SST
anomalies over the Pacific Ocean (60° S–70° N, 110° E–70° W) during 1980–2020 (Meehl et al., 2009). For the model
simulation results, we subtract the global averaged SST time series from the simulated SST patterns prior to the EOF
115 analysis to remove the global warming mode induced by the greenhouse gases (GHG). For ERA5, the detrended SST is
obtained by subtracting the least squares linear trend of the long-term SST (Xu and Hu, 2018). In addition to the EOF based
IPO index, we also use the Triple index for the Interdecadal Pacific Oscillation (TPI) developed by Henley et al. (2015) as
the time evolution of the PDV variation. TPI is defined as the difference in SST anomalies between the central Equatorial
Pacific (10° S–10° N, 170° E–90° W) and the average of the western North Pacific (25°–45° N, 140° E–145° W) and
120 western South Pacific (50°–15° S, 150° E–160° W). A positive (negative) TPI index indicates that the IPO is a positive
(negative) phase. A 13-year Lanczos low-pass filter is applied to the SST anomalies prior to the calculation of IPO and TPI
index to smooth out the high-frequency signals such as ENSO.

In addition to the IPO pattern, the 2nd leading EOF of the observed Pacific SST anomalies shows an inter-hemispheric
125 asymmetry pattern over the eastern tropical Pacific (ETP). To examine whether the regional AA forcings have any impacts
on this asymmetric pattern, we define an ETP Asymmetric index, which is similar to the definition of TPI but calculates the
difference in smoothed SST anomalies between the northeastern Tropical Pacific (0°–20° N, 120° W–100° W) and
southeastern Tropical Pacific (0°–20° S, 120° W–100° W).

3. Results

3.1 Pacific SST responses to AA forcings

Since the 20th century, industrial aerosols generated from fossil fuel sources ("FF"), dominated by sulfate aerosols, have induced an overall net cooling effect globally. However, the emission control in the Western Hemisphere has led to a continuous weakening of the aerosol cooling effects, which effectively induced large-scale sea surface warming over the Northern Hemisphere (NH) since the 1980s. Looking at the spatial pattern of the SST changes (Fig. 2c), significant warming mainly occurs at the NH mid-to-high latitudes, which is consistent with the latitudinal ranges of the emission cut region in the Western Hemisphere. Interestingly, over the extratropical North Pacific, where no local FF aerosol is emitted or removed, there is still a significant warming trend, similar to the North Atlantic (Fig. 2c). This reveals that the FF aerosols not only impact the local climate change over the emission domain but also impose a strong remote influence over the North Pacific. However, based on previous studies (Diao et al., 2021; Kang et al., 2021), the opposite aerosol forcing evolutions from east (continuously cooling) and west (net warming trend due to emission cuts since the 1980s) may play competing roles over the North Pacific, which is what we will separate using the regional forcing simulations mentioned above.

Based on results from the two regional AA experiments (Figs. 2a & b), it is clear that the Pacific SST responds differently to EastFF and WestFF. Over the North Pacific, the EastFF favors a PDO-like warming pattern at a multi-decadal time scale, with tropical Eastern Pacific warming (Fig. 2a). The horseshoe-like SST pattern occurs over the North Pacific, with warming over the eastern part of the North Pacific basin and high latitude while cooling over the western basin of the North Pacific. This is expected due to the advection of aerosols (especially from East Asia) from land to the North Pacific (Fig. 1a) and may also be related to the teleconnection between tropical and extratropical Pacific (Wilcox et al., 2019). The strong horseshoe-like SST pattern in the North Pacific, coupled with counterclockwise wind anomalies, intensifies the Aleutian Low. Smith et al. (2016) argued that the AA forcing originated from East Asia induces large-scale warming in the North Pacific and leads to the weakening of the Aleutian Low, while our results here, however, do not support such an argument. The reason is that only the Aerosol-only experiments from CMIP5 (which is similar to the FF experiment) were used in the previous study. Based on the regional AA forcing experiments, it is clear that the large-scale warming in the North Pacific is not only influenced by the EastFF but also strongly driven by the WestFF (Fig. 2b), which will be discussed in detail later. The extratropical South Pacific also shows a similar pattern as the North Pacific in response to EastFF but with a smaller magnitude. In the Tropical Pacific, EastFF induces a typical El Niño-like SST pattern, with cooling over the Indo-Pacific warm pool and the tropical Indian Ocean while warming over the Central and Eastern Equatorial Pacific. This is consistent with the results of Verma et al. (2019), except that they focused on the SST response induced by volcanic aerosol emissions from Asia. In response to the zonal SST gradient over the tropics, the climatological easterly wind over the equatorial Pacific is significantly weakened by westerly anomalies induced by EastFF (Fig. 2a). Similarly, the equatorial westerlies over the Indian Ocean are also weakened but by a smaller magnitude, effectively weakening the climatological Walker circulation.

The strongest SST cooling induced by EastFF occurs over the North Pacific mid-latitudes far away from the emission domain, which again highlights the importance of aerosol remote forcing over the North Pacific.

165 In contrast to EastFF, WestFF induces large-scale warming over the entire extratropical North Pacific (Fig. 2b), which completely offsets the EastFF-induced cooling and dominates the warming trend captured in the FF case (Fig. 2c). Compared to the North Atlantic warming (the subject of many previous studies), the North Pacific warming induced by WestFF is surprisingly even stronger, indicating the significant teleconnection of WestFF remote forcing onto the North Pacific, which is intuitively "upstream" of the Western Hemisphere. The strong warming due to WestFF also induces local

170 clockwise wind anomalies over the Aleutian low, which also dominates the FF-induced response (Fig. 2c). The WestFF-induced warming pattern in the North Pacific is similar to some internal variability experiments from other extratropical teleconnection experiments in previous studies, which indicated the extratropical teleconnection between the Atlantic and the Pacific (Meehl et al., 2021, Ruprich-Robert et al., 2017).

175 The weakening of aerosol forcing in the Western Hemisphere is widely recognized to contribute to North Atlantic warming or even affecting the AMV (Watanabe and Tatebe 2019; Dong and Sutton 2021; Fiedler and Putrasahan 2021). However, the tropical teleconnection processes emphasized in the previous studies, where North Atlantic warming induces an IPO-like SST pattern over the Tropical Pacific, are completely absent in our simulation results (Fig. 2b), presumably due to the lack of warming over the equatorial Atlantic Ocean that could excite the tropical teleconnection bridge (Wang et al., 2019). This

180 reveals that an accurate and realistic characterization of the latitudinal placements of aerosol forcings determines how it remotely contributes to the North Pacific climate responses.

In the Tropical Pacific, Equatorial SST pattern in response to WestFF shows the greatest warming over the central basin of the Equatorial Pacific and cooling over southeastern basin (Fig. 2b), similar to a central Pacific (CP) type El Niño pattern

185 (different from the typical El Niño-like pattern induced by EastFF in Fig. 2a), which is found to be more frequently occurring in recent decades (Freund et al., 2019). In addition, WestFF also induces inter-hemispheric asymmetry of SST over the eastern tropical Pacific, with significant warming in the northeastern tropical Pacific and slight cooling over the cold tongue region (Fig. 2b), which again is the dominant feature of FF simulation and would be completely missed in the simple linear combination of EastFF and WestFF response (Fig. 2d).

190

Indeed, the linear summation of WestFF and EastFF results presented in Fig. 2d shows significantly greater SST responses over the tropics and Southern Hemisphere compared with actual FF results (Fig. 2c). Similarly, the extratropical North Pacific results in the linear summation largely resembled the EastFF signature (though with overall warmer pattern) while the actual FF results are dominated by WestFF. The Atlantic response appears to be largely consistent, with warming from

195 both EastFF and WestFF. Note that the discrepancy in the tropical and South Pacific between the linear summation and

simulated FF response can also be due to aerosol forcings outside the two focused regions (such as South America and Africa), which also impose a remote impact on these regions (Shi et al., 2022).

3.2 Possible AA impacts in observed Pacific variations

As discussed in Sect. 3.1, EastFF induces an IPO-like SST pattern over the Pacific featuring a positive IPO phase (warming

200   tropical eastern Pacific), while WestFF induces large-scale warming in the extratropical North Pacific and favors CP-type El Niño SST pattern with inter-hemispheric asymmetry in the tropics. Thus, it is important to ask whether and how the regional aerosol forcings might have affected the observed Pacific multi-decadal variations from 1980 to 2020.

Figure 3a–b presents the two leading EOF patterns of the observed SST anomalies from ERA5, in which the leading EOF

205   pattern (Fig. 3a) and the corresponding principal component are defined as the IPO pattern and IPO index, respectively. We note that both the EastFF-induced Pacific SST pattern (Fig. 2a) and the leading EOF pattern of EastFF SST responses (Fig. 3c) resemble the conventional IPO pattern (with an uncentered pattern correlation of 0.43), suggesting that the traditional calculation of IPO can be partly affected by the EastFF. The increasing TPI index induced by EastFF indicates that EastFF favors a positive phase of IPO (blue curve in Fig. 3e; the traditional EOF-defined IPO index resembles the TPI index and

210   thus is not shown). However, the observed IPO shows a transition from positive phase to negative phase from 1980 to 2020 (black curve in Fig. 3e), which is opposite to that induced by EastFF. This suggests that EastFF weakened the negative evolution of the observed IPO in terms of magnitude during this period, but the contribution is small and is overwhelmed by the observed IPO. One thing to be noted here is that the observed IPO is primarily considered to be dominated by the internal variability, although other external forcings (such as volcanic aerosols) might also correspond to the observed transition.

215   Furthermore, the modulation of external forcings to the internal variation is a complicated question, which can also involve the impacts of frequencies, magnitude, and trends. In this study, however, we are primarily focused on the multi-decadal trend of the Pacific SSTs driven by the regional aerosol forcings. Further detailed analyses on the interaction between external forcings (including, but not limited to, aerosol forcings) and internal variability worth more investigation, but are beyond the scope of this study, though.

220

In contrast to the EastFF, WestFF favors an inter-hemispheric asymmetric pattern over ETP, with warming in the NH part while cooling in the SH part (Fig. 2b), which is similar to the second EOF pattern (Fig. 3b; with a pattern correlation of 0.53). Comparing the ETP asymmetric index obtained from ERA5 and WestFF, the WestFF-induced asymmetric response shows the same evolution tendency as the observed variation (Fig. 3f). It is clear that both the WestFF-induced pattern and

225   the second EOF pattern show a CP-type El Niño-like SST pattern in the equatorial Pacific, as well as the inter-hemispheric asymmetry in ETP cold tongue region. This indicates the potential role of WestFF in driving the secondary mode of Pacific variation at decadal to multi-decadal timescales. Recent studies also demonstrate the observed asymmetric changes in ENSO

activities (Jiang and Zhu 2018), which could also be partly affected by the WestFF. However, the interannual variation is beyond the scope of this study.

230 **3.3 Walker circulation responses to AA forcings**

Motivated by the distinct impacts of EastFF versus WestFF on the tropical Pacific SST, here we further examine zonal circulation responses.

Figures 4a and c show the equatorial zonal circulation and precipitation changes in response to EastFF. Induced by the local
235 increasing aerosol emission, the maritime continent receives less surface heat flux (not shown) and weakens the Pacific zonal SST gradient from west to east, concurrent with downward motion anomalies over the maritime continent (Fig. 4a). However, over the Equatorial West Pacific (EWP), where a significant warming signal occurs, there are strong upward motion anomalies along with increases in precipitation. Together, these induce counterclockwise zonal circulation anomalies within the ascending branch of the climatological Pacific Walker circulation (PWC). Over the central and eastern equatorial
240 Pacific (descending branch of PWC), EastFF largely induces weak upward motion anomalies, effectively leading to the weakening of PWC. Overall, although having a similar SST pattern with the El Niño events, EastFF induces a weakening of PWC but with the strongest impact *within* the ascending branch by shifting the ascending center eastward. As a minor note, EastFF also induces weak descending motion over the equatorial Atlantic Ocean by inducing trans-basin westerlies at a higher level, and thus weakens the Atlantic Walker circulation (AWC; Fig. 4a). This is consistent with the tropical
245 teleconnection pathway between the tropical Pacific and tropical Atlantic (e.g., Meehl et al., 2021).

Despite being a remote forcing, WestFF induces very similar zonal circulation changes over the Indo-Pacific warm pool region compared to EastFF (Fig. 4b). This is consistent with the CP-type El Niño pattern (Fig. 2b) with a positive SST zonal gradient within the Indo-Pacific warm pool regions. However, the WestFF response shows opposite circulation changes in
250 the descending branch of climatological PWC, which strengthens the downward motion and suppresses the local rainfall (Fig. 4d). Consistent with the latitudinally asymmetric SST pattern over the eastern Equatorial Pacific (Fig. 2b), the Walker Circulation and precipitation responses also feature asymmetric changes with a northward shift. Overall, the WestFF enhances the strength of the PWC and slightly shifts the ascending center of the PWC eastward. Surprisingly, the WestFF does not induce any noticeable Walker circulation changes over the equatorial Atlantic, despite the warming trend over the
255 tropical/subtropical Atlantic Ocean (Fig. 2c). This further indicates that the tropical Pacific responses to WestFF are not facilitated by the tropical teleconnection pathway. The zonal gradient of SST between the Indo-Pacific warm pool and the eastern basin of the Equatorial Pacific is commonly utilized to indicate the strength of PWC. However, the zonal gradient cannot fully indicate the changes in PWC induced by regional aerosol forcings because of the zonal shift of the ascending branch of PWC. This implies the importance of considering the zonal placement of radiative forcing, especially for short-
260 lived aerosol forcings.

3.4 Distinct teleconnection mechanisms in driving the North Pacific

As demonstrated in Sect. 3.1, the extratropical North Pacific has the largest warming in response to aerosol forcings remotely. Both EastFF and WestFF contribute to the warming in the eastern North Pacific but offset each other over the western basin of the North Pacific. This brings the question of whether and how the East and West aerosol forcings affect the

265 North Pacific climate pattern differently. Previous studies have demonstrated the teleconnections between the Pacific and Atlantic as well as the connections between the tropical and extratropical Pacific, but most of these studies are in the context of understanding the internal variability of the Pacific or the Atlantic (Wang 2019; Kang et al., 2021; Meehl et al., 2021; Yao et al., 2021). Here, we aim to demonstrate a unique mechanism of how regional aerosols affect the North Pacific mid-latitude climate remotely.

270

Figure 5 shows the upper troposphere eddy geopotential height (Z200e) and stream function changes in response to the regional FF forcings and the corresponding sea level pressure (SLP) changes. The EastFF-induced radiative cooling over the Indo-Pacific warm pool increases the local SLP, which leads to the weakening of PWC (Fig. 4a) and westerly wind anomalies at the near-surface level. As a result, the readjustment of PWC and low-level wind excites an El-Nino-like SST

275 pattern over the tropical Pacific (Fig. 2a), which excites a Rossby wave train from tropics to extratropic (Fig. 5a). The enhanced convection over the central Equatorial Pacific (Fig. 4a) leads to anomalous upper-level high in the tropical North and South Pacific, and anomalous upper-level low over the extratropical North Pacific (Fig. 5a). Correspondingly, as a barotropic system, the SLP also shows anomalous low over the North Pacific and cyclonic near-surface wind anomalies (Fig. 5c). As another contributing factor, the emitted aerosols over East Asia (Fig. 1a) are transported to the western basin of

280 North Pacific (Diao et al., 2021; Xiang et al., 2023), which induces cooling effects and further enhances the low-level westerly wind anomalies in the subtropical North Pacific (Boo et al., 2015; Chung and Soden, 2017). The intensified westerly wind at the mid-latitudes increases the surface heat flux and, thus, induces a cooling response over the western North Pacific, following the wind-evaporation-SST (WES) feedback (Xie 1996). This explains why EastFF induces the IPO-like pattern over the extratropical North Pacific region; indeed, the mechanism here in the EastFF case largely resembles the

285 classic ENSO teleconnection originating from the tropical and propagating into extratropical Pacific, but here manifesting at a multi-decadal time scale.

Next, we show that the patterns of surface and upper-level convection in response to WestFF are remarkably different from those in response to EastFF, where no obvious upper-level wave activity is found in the tropics (Fig. 5d). The radiative

290 heating in the Western Hemisphere mid-latitude area excites wave trains propagating into the NH mid-latitudes, resulting in anomalous upper-level high over the extratropical North Pacific (Fig. 5d). As a result, SLP rises over the eastern North Pacific (Fig. 5f), with anticyclonic near-surface wind anomalies. In contrast to the EastFF response, such anomalous easterlies in the mid-latitudes surface weaken climatological westerly wind, reducing the energy advection via WES

feedback (Sun et al., 2017; Wang 2019). This can amplify the significant warming over the eastern basin of the North Pacific

295   in response to WestFF.

Some previous studies demonstrated that the North Atlantic warming remotely impacts the North Pacific via the tropical connections between the Atlantic and the Pacific (Sun et al., 2017; Johnson et al., 2020; Meehl et al., 2021). However, the tropical teleconnection pathway does not seem to be in play in the WestFF case given that there are no significant Atlantic

300   Walker circulation changes (Fig. 4b) or geopotential height perturbations over the tropical Pacific (Fig. 5d). The mid-latitude teleconnection pathway invoked by WestFF aerosol forcing that we propose here is less discussed in previous studies. We argue that this west-to-east mid-latitude pathway is the dominant pathway for the perturbations introduced by regional forcing placed at higher latitudes.

305   This sensitivity to the latitudinal displacement of forcing is supported by our secondary analysis of biomass burning-related aerosol experiment (BMB), in which one major aerosol forcings are located in northeastern Asia in this particular model experiment (Fig. 2 in Diao et al., 2021), and we find similar wave trains propagating in the mid-latitudes (Fig. 6). Similarly, in some other model experiments, the Atlantic heating, when placed in the extratropical, regardless of internal variability (Yao et al., 2021) or external forcings (Ruprich-Robert et al., 2017), does not excite the tropical teleconnection pathway.

310   This further highlights the sensitive role of the latitudinal location of forcings.

In summary, although EastFF and WestFF both remotely drive the long-term SST changes in the North Pacific, due to the different latitudinal locations of the forcings, there are remarkably different teleconnection pathways. Therefore, the decadal changes in the North Pacific SST could be hard to understand if only looking at the total aerosol forcing experiments.

315   **4. Conclusion**

Since the 1980s, the radiative forcing due to industrial-related aerosol emission has shown opposite emission trends over the Eastern and Western Hemisphere (Kang et al., 2021). Using a set of large ensemble transient simulations, we find that aerosol forcings in both the eastern and the western Hemispheres can induce multi-decadal climate responses over the tropical and extratropical North Pacific but with distinct mechanisms.

320

Over the tropical Pacific, EastFF (cooling trend) induces a typical El Niño-like SST pattern and anomalous westerly wind over the tropical Pacific. Corresponding to the adjustment of the equatorial SST gradient, EastFF drives an eastward shift of the ascending branch of the PWC and an upwelling motion anomaly in the descending branch of the PWC, which effectively weakens the overall strength of the climatological PWC. In contrast, WestFF (net warming trend since the 1980s) induces a

325   CP-type El Niño-like SST pattern in the tropical Pacific with the most profound warming over the western and central

equatorial Pacific but cooling over the eastern equatorial Pacific. At the same time, the eastern equatorial Pacific also shows inter-hemispheric asymmetry in response to WestFF, which resembles the 2nd EOF pattern of the Pacific SST changes. WestFF drives an eastward shift of the ascending branch of the PWC, which is similar to EastFF but strengthens the broader descending branch of the PWC.

330

EastFF imposes a positive IPO-like pattern onto the Pacific. However, the observational IPO during 1980–2020 features a shift to the negative phase, which indicates that internal variability is the dominant driver of the observed IPO pattern. This suggests the EastFF-induced positive IPO pattern partly offsets the internal variability from 1980 to 2020. The inter-hemispheric asymmetry pattern (stronger warming in the North Pacific) driven by WestFF resembles the 2nd leading EOF
335   pattern of the Pacific SST changes, suggesting that WestFF at least partly contributes to the observed asymmetric pattern over the Eastern Tropical Pacific during 1980-2020.

In the extratropical North Pacific, which is the focus of this study, EastFF leads to a positive IPO-like SST pattern, with cooling over the western part and warming over the eastern part. In contrast, WestFF induces large-scale warming in the
340   North Pacific, which is even stronger than in the North Atlantic. This warming almost completely offsets the cooling driven by EastFF in the overall FF case. EastFF remotely drives the North Pacific following the typical ENSO teleconnection pathway between tropical and extratropical Pacific but at a multi-decadal time scale. The commonly discussed tropical bridge pathway between the Atlantic and the Pacific is not found to be important in the WestFF responses. Instead, we show that WestFF excites the North Pacific responses via a mid-latitude teleconnection pathway, which has been discussed less in
345   previous studies. The distinction of teleconnection mechanisms is because the WestFF forcings are located at higher latitudes (Diao et al., 2021). This argument is supported by the result of the BMB aerosol forcing experiment, which is displaced even further in the higher latitude in NH (Fig. 6). This further suggests the importance of the latitudinal location of the aerosol forcings.

350   In this study, we focus on the period of 1980–2020, when aerosol emissions over Asia show an overall increasing trend. However, studies have shown that the emission from East Asia reached a peak around the 2010s and started to decline recently while South Asia emission continues to increase (Samset et al., 2019; Wang et al., 2021). The sensitivity of aerosol forcing's latitudinal placement within Asia is also highlighted by recent studies on dipole patterns emerging in Asia (Wang et al., 2022; Xiang et al., 2023). Also, the current offsetting effects between EastFF and WestFF can flip to a joint effect over
355   specific regions of the North Pacific in the coming few decades. Such decline and/or redistribution of aerosol emissions can lead to distinct climate responses locally and remotely, which demands further continuous investigation in the future.
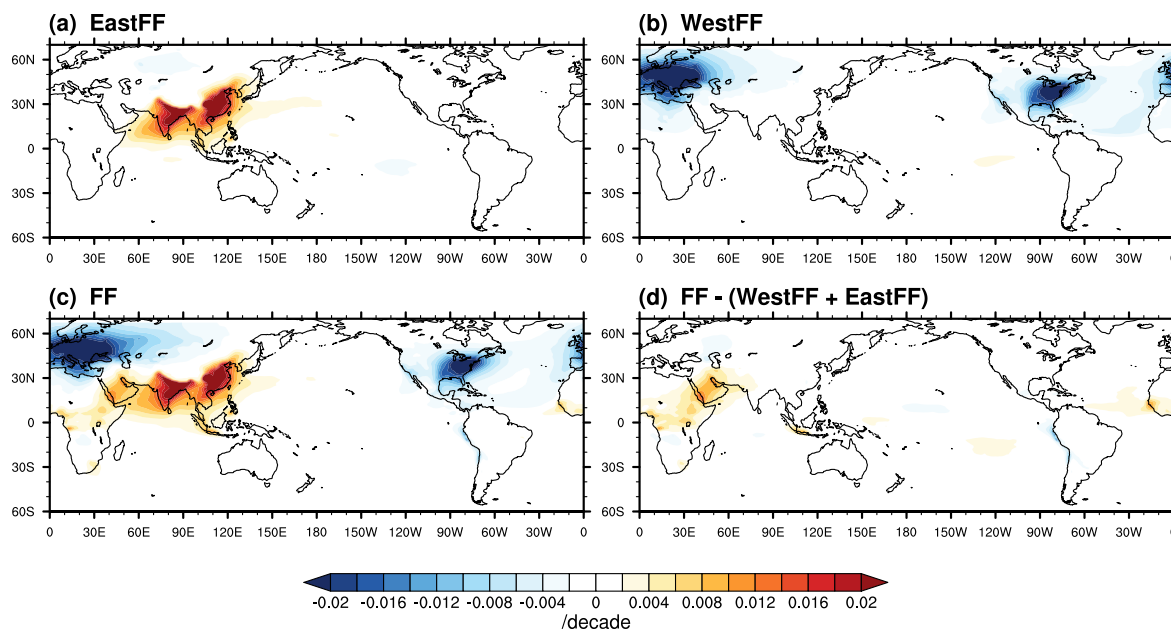
Figure 1

360 Decadal trends in anthropogenic aerosol optical depth at 550 nm (AOD-AA; 1 per decade) during 1980–2020 in response to (a) EastFF, (b) WestFF, and (c) FF. AOD-AA is calculated by subtracting the dust AOD from the total AOD. (d) The difference between FF-induced AOD changes and the combination of AOD changes induced by EastFF and WestFF.
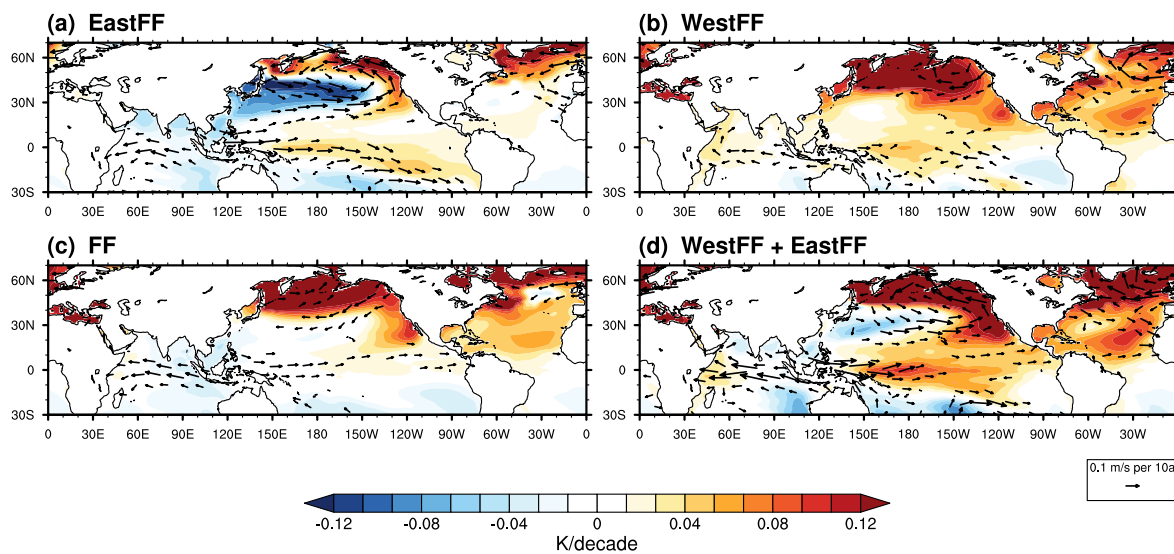
Figure 2

(a) Decadal changes in sea surface temperature (shading; K per decade) and 850 hPa horizontal wind (vectors; m s^{-1} per decade) during 1980–2020 calculated in response to EastFF. (b) and (c): As in (a), but showing results for WestFF and FF, respectively. (d) Linear addition of panels (a) and (b).
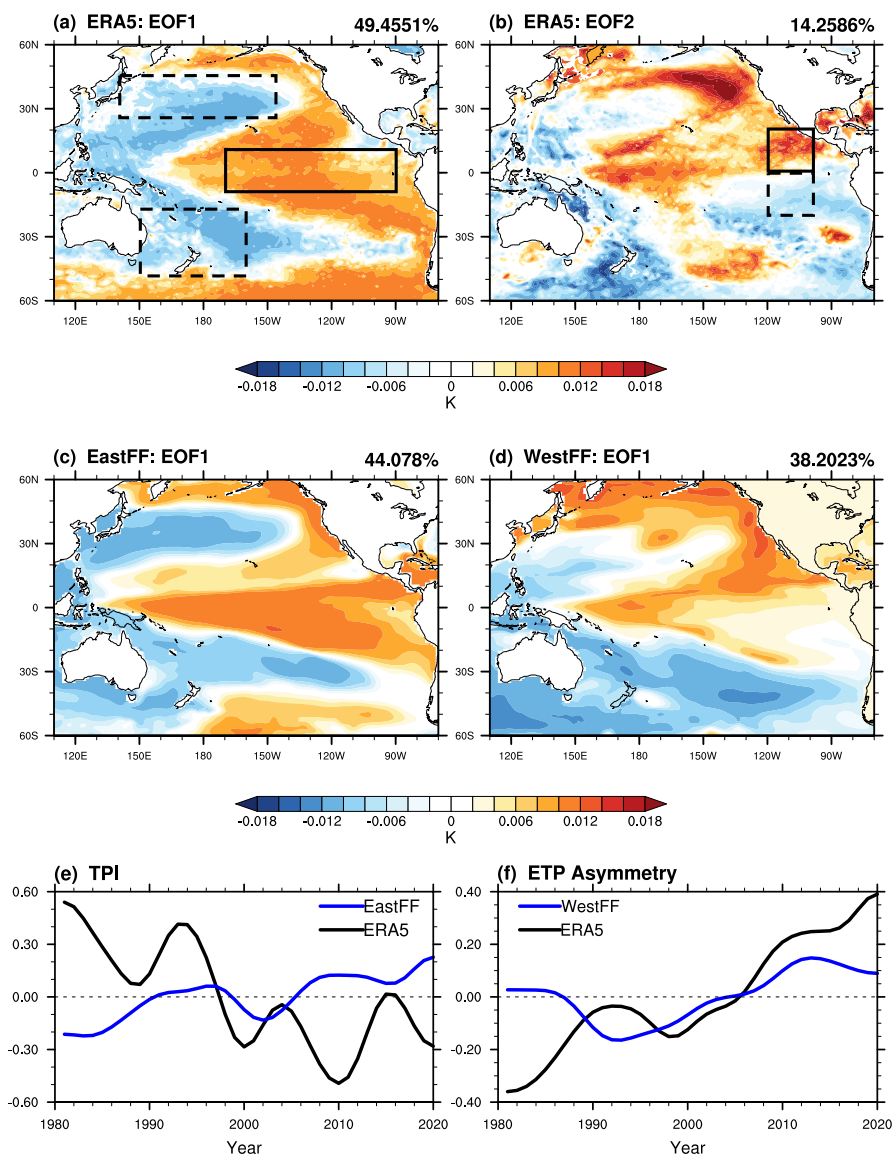
Figure 3

(a–b) The 1st and 2nd leading empirical orthogonal function (EOF) patterns of the observed SST anomalies from ERA5 over the Pacific Ocean during 1980–2020. boxes in panel (a) represent the three key regions used to calculate the TPI index; boxes in panel (b) represent the two key regions used to calculate the ETP asymmetry index (described in Sect. 2.3); (c) The leading EOF pattern of the ensemble-mean SST responses from EastFF; (d) as in (c) but for WestFF result; (e) The time series of TPI index obtained from (black) ERA5 and (blue) EastFF; (f) The time series of ETP asymmetry index obtained from (black) ERA5 and (blue) WestFF.
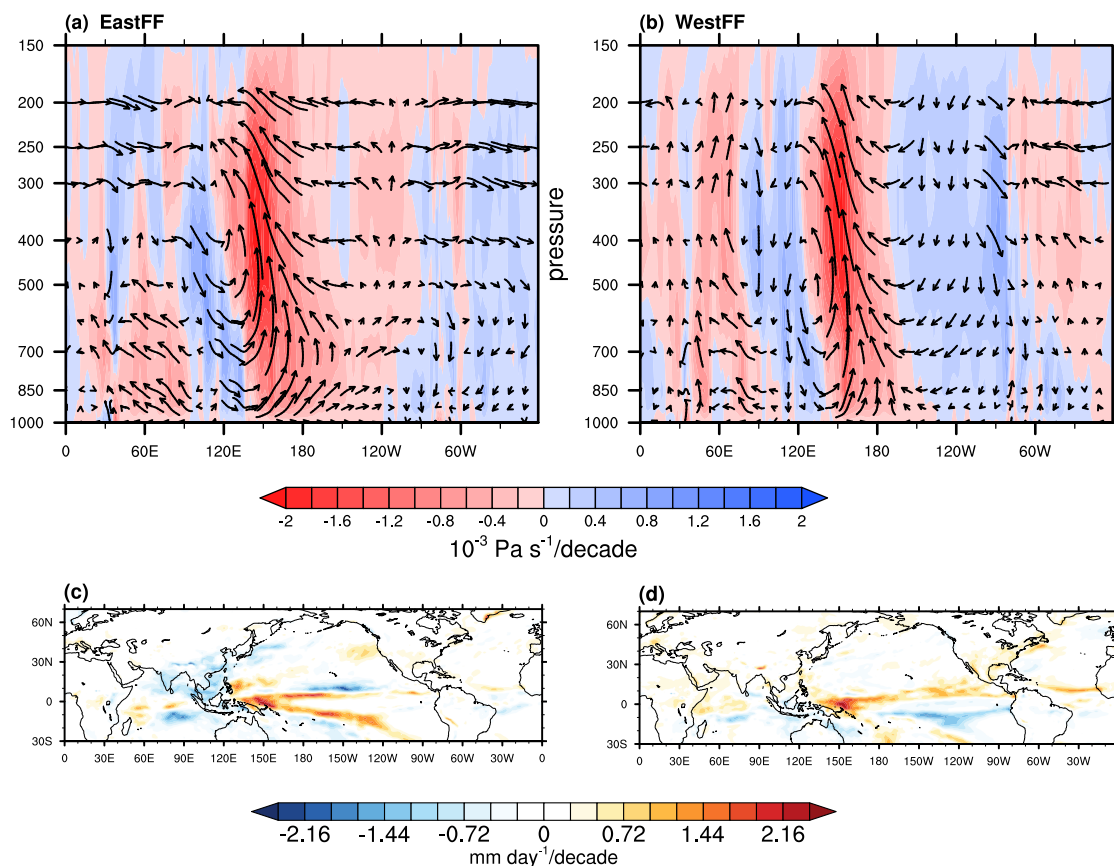
Figure 4 Changes in the tropical circulation.

(a) Decadal changes in cross-section of winds averaged from 5° S–5° N (vectors; The vertical component of the velocity vectors is scaled by a factor of 300) and vertical motion (shading; Pa s-1 in response to EastFF. Blue shading indicates downward motions; red shading indicates upward motions). (b) As in panel (a) but for WestFF. (c) Changes in tropical Precipitation (mm day-1 per decade) in response to EastFF. (d) As in (c), but for WestFF.
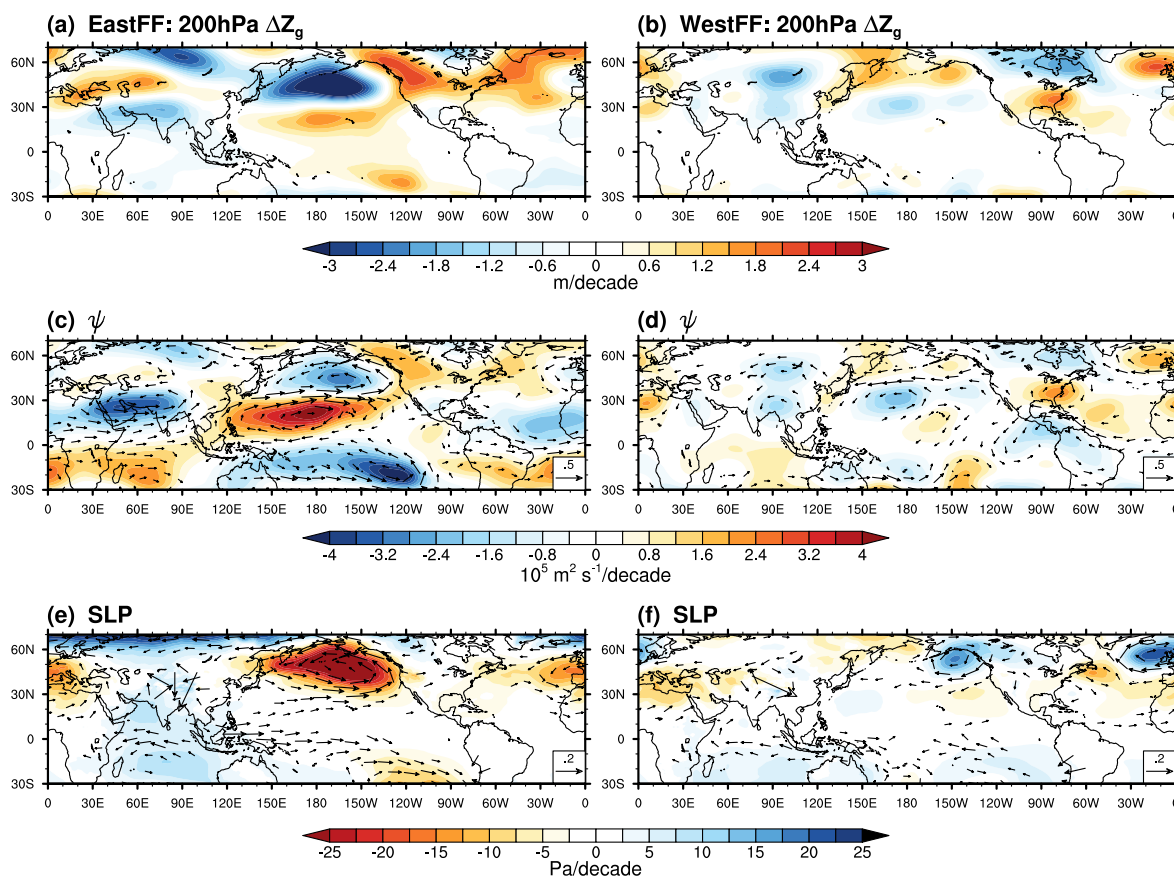
Figure 5

Left panels: EastFF-induced decadal changes of (a) 200 hPa eddy geopotential height (m per decade), (c) 250 hPa stream function (shading; m2 s-1 per decade), and wind (vectors; m s-1 per decade), and (e) sea level pressure (shading; Pa per decade) and 850 hPa low-level wind (vectors; m s-1 per decade). Right panels: same as Left panels, but due to WestFF.
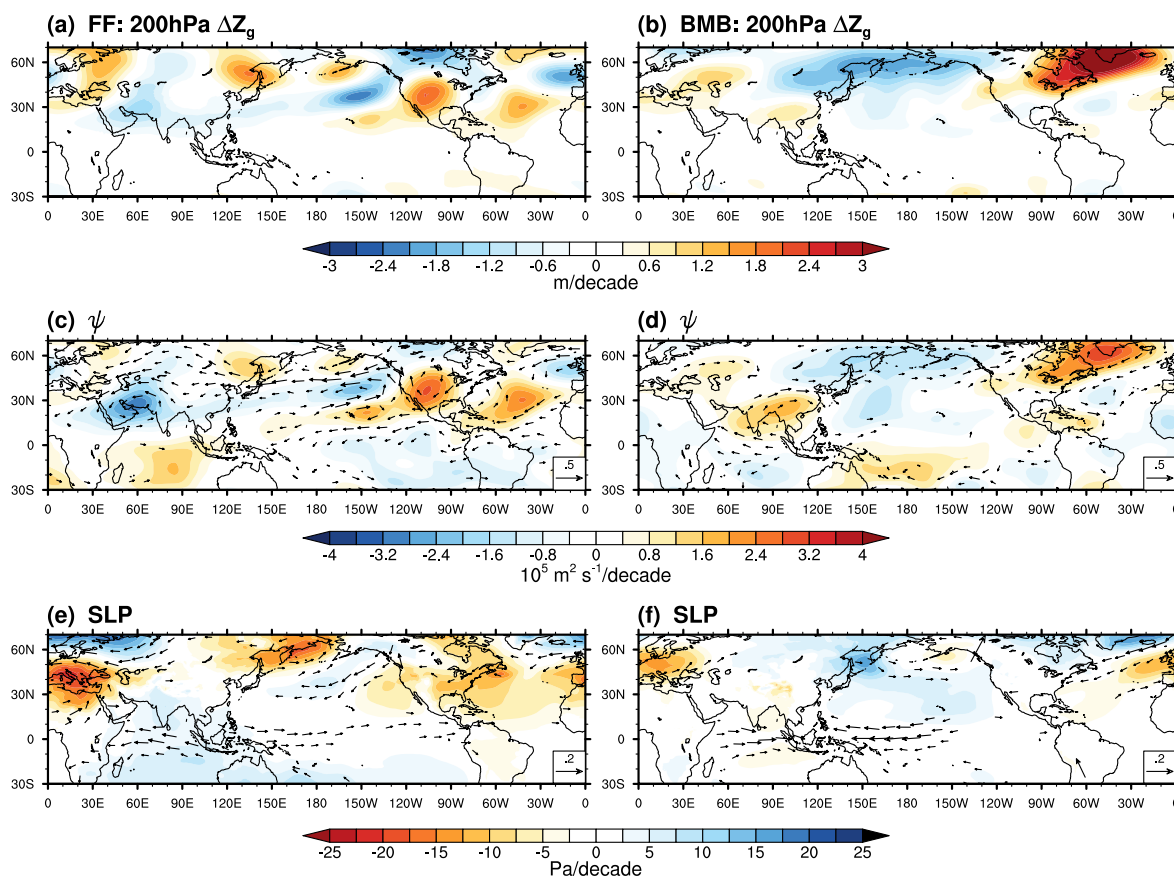
Figure 6

Left panels: FF-induced decadal changes (1980–2020) of (a) 200 hPa eddy geopotential height (m per decade), (c) 250 hPa
395   stream function (shading; m^2 s^{-1} per decade), and wind (vectors; m s^{-1} per decade), and (e) sea level pressure (shading; Pa per
decade) and 850 hPa low-level wind (vectors; m s^{-1} per decade). Right panels: same as Left panels, but due to Biomass
burning (BMB) simulations.

Code/Data availability

400   Datasets of the CESM1 Large Ensemble Project are available from: https://www.cesm.ucar.edu/projects/community-projects/LENS/data-sets.html (last access: 21 June 2024; Kay et al., 2015). Datasets of the CESM1 "Single Forcing" Large Ensemble Project are available from: https://www.cesm.ucar.edu/working_groups/CVC/simulations/cesm1-single_forcing_le.html (last access: 21 June 2024; Deser et al., 2020). Outputs for the two sets of regional single-forcing large-ensemble (Fix_EastFF1920 and Fix_WestFF1920; Diao et al., 2021) are available on the National Center for

405   Atmospheric Research (NCAR) Campaign Storage file system and can also be accessed via the NCAR Data Sharing Service Endpoint on Globus upon request to the authors. All data analysis codes related to this study are available at: https://github.com/C-R-Diao/Climo_Pacific_reg-AA.git. At the time of publication, the codes will be converted to a permanent repository.

Author contribution

410   CD and YX developed the idea for this study. CD performed the code development the data analyses, with input and feedback from YX, ZW, and AH. CD and YX prepared the paper, with contributions from all authors.

Competing interests

The contact author has declared that neither they nor their co-authors have any competing interests.

Acknowledgements

415   This work is supported by the National Science Foundation (NSF, grant no. 841308). We acknowledge NCAR for the high-performance computing support from Cheyenne (https://doi.org/10.5065/D6RX99HX) and the data storage resources provided by Computational and Information Systems Laboratory (CISL), sponsored by the National Science Foundation. We thank the CESM-LE project and the CESM1 Single Forcing Large Ensemble Project for providing access to the model outputs.

420

References

Allen, R. J., Norris, J. R., & Kovilakam, M. (2014). Influence of anthropogenic aerosols and the Pacific Decadal Oscillation on tropical belt width. *Nature Geoscience*, *7*(4), 270–274. https://doi.org/10.1038/ngeo2091

425 Bellomo, K., Murphy, L. N., Cane, M. A., Clement, A. C., & Polvani, L. M. (2018). Historical forcings as main drivers of the Atlantic multidecadal variability in the CESM large ensemble. *Climate Dynamics*, *50*(9), 3687–3698. https://doi.org/10.1007/s00382-017-3834-3

Boo, K.-O., Booth, B. B. B., Byun, Y.-H., Lee, J., Cho, C., Shim, S., & Kim, K.-T. (2015). Influence of aerosols in multidecadal SST variability simulations over the North Pacific. *Journal of Geophysical Research: Atmospheres*, *120*(2),

430 517–531. https://doi.org/https://doi.org/10.1002/2014JD021933

Booth, B. B. B., Dunstone, N. J., Halloran, P. R., Andrews, T., & Bellouin, N. (2012). Aerosols implicated as a prime driver of twentieth-century North Atlantic climate variability. *Nature*, *484*(7393), 228–232. https://doi.org/10.1038/nature10946

Chung, E.-S., & Soden, B. J. (2017). Hemispheric climate shifts driven by anthropogenic aerosol–cloud interactions. *Nature Geoscience*, *10*(8), 566–571. https://doi.org/10.1038/ngeo2988

435 Deser, C., Phillips, A. S., Simpson, I. R., Rosenbloom, N., Coleman, D., Lehner, F., et al. (2020). Isolating the Evolving Contributions of Anthropogenic Aerosols and Greenhouse Gases: A New CESM1 Large Ensemble Community Resource. *Journal of Climate*, *33*(18), 7835–7858. https://doi.org/10.1175/JCLI-D-20-0123.1

Diao, C., Xu, Y., & Xie, S.-P. (2021). Anthropogenic aerosol effects on tropospheric circulation and sea surface temperature (1980–2020): separating the role of zonally asymmetric forcings. *Atmospheric Chemistry and Physics*, *21*(24), 18499–

440 18518. https://doi.org/10.5194/acp-21-18499-2021

Dittus, A. J., Hawkins, E., Robson, J. I., Smith, D. M., & Wilcox, L. J. (2021). Drivers of Recent North Pacific Decadal Variability: The Role of Aerosol Forcing. *Earth's Future*, *9*(12), 1–15. https://doi.org/10.1029/2021EF002249

Dong, L., Zhou, T., & Chen, X. (2014). Changes of Pacific decadal variability in the twentieth century driven by internal variability, greenhouse gases, and aerosols. *Geophysical Research Letters*. https://doi.org/10.1002/2014GL062269

445 Freund, M. B., Henley, B. J., Karoly, D. J., McGregor, H. V, Abram, N. J., & Dommenget, D. (2019). Higher frequency of Central Pacific El Niño events in recent decades relative to past centuries. *Nature Geoscience*, *12*(6), 450–455. https://doi.org/10.1038/s41561-019-0353-3

Hassan, T., Allen, R. J., Liu, W., & Randles, C. A. (2021). Anthropogenic aerosol forcing of the Atlantic meridional overturning circulation and the associated mechanisms in CMIP6 models. *Atmos. Chem. Phys.*, *21*(8), 5821–5846.

450 https://doi.org/10.5194/acp-21-5821-2021

Henley, B. J., Gergis, J., Karoly, D. J., Power, S., Kennedy, J., & Folland, C. K. (2015). A Tripole Index for the Interdecadal Pacific Oscillation. *Climate Dynamics*, *45*(11), 3077–3090. https://doi.org/10.1007/s00382-015-2525-1

Hersbach, H., Bell, B., Berrisford, P., Biavati, G., Horányi, A., Muñoz Sabater, J., Nicolas, J., Peubey, C., Radu, R., Rozum, I., Schepers, D., Simmons, A., Soci, C., Dee, D., Thépaut, J-N. (2023): ERA5 monthly averaged data on single levels from

455   1940 to present. Copernicus Climate Change Service (C3S) Climate Data Store (CDS), DOI: 10.24381/cds.f17050d7

Hua, W., Dai, A., & Qin, M. (2018). Contributions of Internal Variability and External Forcing to the Recent Pacific Decadal Variations. *Geophysical Research Letters*, *45*(14), 7084–7092. https://doi.org/10.1029/2018GL079033

Hua, W., Dai, A., Zhou, L., Qin, M., & Chen, H. (2019). An Externally Forced Decadal Rainfall Seesaw Pattern Over the Sahel and Southeast Amazon. *Geophysical Research Letters*, *46*(2), 923–932. https://doi.org/10.1029/2018GL081406

460   Huang, B., Thorne, P. W., Banzon, V. F., Boyer, T., Chepurin, G., Lawrimore, J. H., et al. (2017). Extended Reconstructed Sea Surface Temperature, Version 5 (ERSSTv5): Upgrades, Validations, and Intercomparisons. *Journal of Climate*, *30*(20), 8179–8205. https://doi.org/10.1175/JCLI-D-16-0836.1

Hurrell, J. W., Holland, M. M., Gent, P. R., Ghan, S., Kay, J. E., Kushner, P. J., et al. (2013). The Community Earth System Model: A Framework for Collaborative Research. *Bulletin of the American Meteorological Society*, *94*(9), 1339–1360.

465   https://doi.org/10.1175/BAMS-D-12-00121.1

IPCC. (2018). *IPCC Special Report on the impacts of global warming of 1.5°C. Ipcc - Sr15*.

Johnson, Z. F., Chikamoto, Y., Wang, S.-Y. S., McPhaden, M. J., & Mochizuki, T. (2020). Pacific decadal oscillation remotely forced by the equatorial Pacific and the Atlantic Oceans. *Climate Dynamics*, *55*(3), 789–811. https://doi.org/10.1007/s00382-020-05295-2

470   Kang, S. M., Xie, S.-P., Deser, C., & Xiang, B. (2021). Zonal mean and shift modes of historical climate response to evolving aerosol distribution. *Science Bulletin*. https://doi.org/https://doi.org/10.1016/j.scib.2021.07.013

Kay, J. E., Deser, C., Phillips, A., Mai, A., Hannay, C., Strand, G., et al. (2015). The Community Earth System Model (CESM) Large Ensemble Project: A Community Resource for Studying Climate Change in the Presence of Internal Climate Variability. *Bulletin of the American Meteorological Society*, *96*(8), 1333–1349. https://doi.org/10.1175/BAMS-D-13-

475   00255.1

Lin, L., Xu, Y., Wang, Z., Diao, C., Dong, W., & Xie, S.-P. (2018). Changes in Extreme Rainfall Over India and China Attributed to Regional Aerosol-Cloud Interaction During the Late 20th Century Rapid Industrialization. *Geophysical Research Letters*, *45*(15), 7857–7865. https://doi.org/10.1029/2018GL078308

Meehl, G. A., Hu, A., & Santer, B. D. (2009). The Mid-1970s Climate Shift in the Pacific and the Relative Roles of Forced

480   versus Inherent Decadal Variability. *Journal of Climate*, *22*(3), 780–792. https://doi.org/10.1175/2008JCLI2552.1

Meehl, G. A., Hu, A., Castruccio, F., England, M. H., Bates, S. C., Danabasoglu, G., et al. (2021). Atlantic and Pacific tropics connected by mutually interactive decadal-timescale processes. *Nature Geoscience*, *14*(1), 36–42. https://doi.org/10.1038/s41561-020-00669-x

Ming, Y., & Ramaswamy, V. (2011). A Model Investigation of Aerosol-Induced Changes in Tropical Circulation. *Journal of*

485   *Climate*, *24*(19), 5125–5133. https://doi.org/10.1175/2011JCLI4108.1

Ramanathan, V., Crutzen, P. J., Kiehl, J. T., & Rosenfeld, D. (2001). Aerosols, Climate, and the Hydrological Cycle. *Science*, *294*(5549), 2119–2124. https://doi.org/10.1126/science.1064034

Ruprich-Robert, Y., Msadek, R., Castruccio, F., Yeager, S., Delworth, T., & Danabasoglu, G. (2017). Assessing the Climate Impacts of the Observed Atlantic Multidecadal Variability Using the GFDL CM2.1 and NCAR CESM1 Global Coupled Models. *Journal of Climate*, *30*(8), 2785–2810. https://doi.org/10.1175/JCLI-D-16-0127.1

Samset, B. H., Lund, M. T., Bollasina, M., Myhre, G., & Wilcox, L. (2019). Emerging Asian aerosol patterns. *Nature Geoscience*, *12*(8), 582–584. https://doi.org/10.1038/s41561-019-0424-5

Shi, J.-R., Kwon, Y.-O., & Wijffels, S. E. (2022). Two Distinct Modes of Climate Responses to the Anthropogenic Aerosol Forcing Changes. *Journal of Climate*, *35*(11), 3445–3457. https://doi.org/10.1175/JCLI-D-21-0656.1

Shindell, D. T., Faluvegi, G., Rotstayn, L., & Milly, G. (2015). Spatial patterns of radiative forcing and surface temperature response. *Journal of Geophysical Research: Atmospheres*, *120*(11), 5385–5403. https://doi.org/doi:10.1002/2014JD022752

Smith, D. M., Booth, B. B. B., Dunstone, N. J., Eade, R., Hermanson, L., Jones, G. S., et al. (2016). Role of volcanic and anthropogenic aerosols in the recent global surface warming slowdown. *Nature Climate Change*, *6*(10), 936–940. https://doi.org/10.1038/nclimate3058

Sun, C., Kucharski, F., Li, J., Jin, F.-F., Kang, I.-S., & Ding, R. (2017). Western tropical Pacific multidecadal variability forced by the Atlantic multidecadal oscillation. *Nature Communications*, *8*(1), 15998. https://doi.org/10.1038/ncomms15998

Verma, T., Saravanan, R., Chang, P., & Mahajan, S. (2019). Tropical Pacific Ocean Dynamical Response to Short-Term Sulfate Aerosol Forcing. *Journal of Climate*, *32*(23), 8205–8221. https://doi.org/10.1175/JCLI-D-19-0050.1

Wang, C. (2019). Three-ocean interactions and climate variability: a review and perspective. *Climate Dynamics*, *53*(7–8), 5119–5136. https://doi.org/10.1007/s00382-019-04930-x

Wang, C., Z. Wang, Y. Lei, H. Zhang, H. Che, and X. Zhang (2022), Differences in East Asian summer monsoon responses to Asian aerosol forcing under different emission inventories, Adv. *Clim. Chang. Res.,* 13(3), 309-322, doi:10.1016/j.accre.2022.02.008

Wang, Z., Lin, L., Xu, Y., Che, H., Zhang, X., Zhang, H., et al. (2021). Incorrect Asian aerosols affecting the attribution and projection of regional climate change in CMIP6 models. *Npj Climate and Atmospheric Science*, *4*(1), 2. https://doi.org/10.1038/s41612-020-00159-2

Watanabe, M., & Tatebe, H. (2019). Reconciling roles of sulphate aerosol forcing and internal variability in Atlantic multidecadal climate changes. *Climate Dynamics*, *53*(7), 4651–4665. https://doi.org/10.1007/s00382-019-04811-3

Xie, S.-P. (1996). Westward Propagation of Latitudinal Asymmetry in a Coupled Ocean–Atmosphere Model. *Journal of Atmospheric Sciences*, *53*(22), 3236–3250. https://doi.org/10.1175/1520-0469(1996)053<3236:WPOLAI>2.0.CO;2

Yao, B., Xu, Y., Dessler, A. E., & Liu, C. (2021). Characterizing unforced decadal climate variability in global climate model large ensembles. *Climate Dynamics*. https://doi.org/10.1007/s00382-021-05900-y